# Deflection Measurements Using Moiré Gap Effect

by

Fu-pen Chiang, Assistant Professor
and
Belthur Ranganayakamma, Graduate Student

Department of Mechanics
College of Engineering

State University of New York at Stony Brook

Report No. 152

January 1970

## Abstract

The moiré gap equation originally derived by Sciammarella and Chiang has been generalized to include linear and rotational mismatches. The equation is then applied to the measurement of deflection of beams and plates. The method has the advantages of being simple in comparison with other optical whole-field methods. The application of moiré gap effect to the study of dynamic problems is also discussed.

Introduction:

It is well known that there are basically two types of moiré fringes created by the superposition of two gratings; namely that due to the difference in pitch and that due to the difference in orientation. And they have been effectively used for two dimensional strain analysis [1, 2, 3, 4]. A third type of moiré fringes which is less familiar to most people is the one created by the presence of a gap between two gratings [5]. Indeed, if two identical gratings are oriented with lines parallel to each other but with a uniform gap between them, one would observe a pattern of uniformly spaced parallel straight fringes running along the direction of the grating lines; and the spacing between the fringes will vary as one varies the distance of observation. The fringe spacing will also vary if one varies the gap between the gratings. These fringes will fade away as the gap becomes too large. The explanation of the phenomenon is the following: Because of the presence of a gap these two gratings are located at different distances from the eye which acts as a lens. As a result, they appear at the retina (the image plane) with different pitches due to the difference in magnification. These two images of the grating will interfere with each other to form a set of fringes equivalent to that formed by two parallel gratings of different pitches in close contact [4]. It is obvious that the appearance of the fringe pattern is a function of the gap as well as the observing distance because both of them contribute to the change of magnification. When the gap is too large so that the two gratings cannot be resolved simultaneously with reasonable sharpness, the interference phenomenon disappears. Presented in the paper is a generalized moiré gap equation and its application to the measurement of deflection of structures. Also presented is the discussion of the possibility of using moiré gap effect for the measurement of dynamical deflections.

## Generalized Moiré Gap Equation

Based on the concept of difference in magnification of two gratings Sciammarella and Chiang [5] derived a moiré-gap-equation giving the relationship between the gap and the fictitious strain thus created in terms of moiré fringes. In the derivation the two gratings were assumed to have identical pitch and are parallel in orientation. In the following the moiré-gap-equation will be generalized to include the presence of linear and rotational mismatches.

If two gratings with a gap between them are placed in front of a camera whose optical axis is perpendicular to the plane of the master grating and the camera is focused on the master grating, they will appear at the image plane of the camera as shown in Fig. 1. Let $p$ and $p'$ denote the pitches of master grating and model grating, respectively; and $\lambda = \frac{p}{p'}$ , linear mismatch; $\theta(0 \leq \theta < \pi/2)$, rotational mismatch, it is easily seen that the effective pitch, before the imaging process, of the model grating in the direction normal to the master grating-lines is given by

$$\frac{p'}{\cos\theta} = \frac{p}{\lambda \cos\theta} \tag{1}$$

After going through the camera lens, the pitch of the master grating at the image plane is given by

$$p_i = p\,\frac{\bar{z}}{z} \tag{2}$$

in which $z$ and $\bar{z}$ are the object and image distances, respectively. And the effective pitch of the model grating at the image plane is given by

$$p_i' = \frac{p}{\lambda \cos\theta}\,\frac{\bar{z}}{z+\Delta z} \tag{3}$$

The relative displacement in terms of moiré fringe order is then

$$N = \left(\frac{1}{p_i} - \frac{1}{p_i'}\right) r \tag{4}$$

where $r$ is the distance measured from the optical axis along the direction normal to master grating-lines (i.e. the principal direction). Because of the axial symmetric property of a lens the principal direction can be oriented arbitrarily in a plane normal to the optical axis. Substituting eqs. (2) and (3) into eq. (4), one obtains

$$N = \frac{r}{pz}[z(1-\lambda\cos\theta) - \Delta z(\lambda\cos\theta)] \tag{5}$$

The fictitious displacement in the direction of $r$ is therefore

$$u_r = Np_i \tag{6}$$

Using eqs. (2) and (6) one obtains

$$u_r = \frac{r}{z}[z(1-\lambda\cos\theta) - \Delta z(\lambda\cos\theta)] \tag{7}$$

when $\lambda = 1$ and $\theta = 0$, eq. (7) reduces to eq. (22) derived in reference [5].

With the presence of a gap a fictitious strain field is introduced and this should be subtracted from the final moire pattern. The magnitude of the fictitious strain field can be obtained by direction $r$ to the direction of $x$ and $y$ consecutively and compute the partial derivatives using eq. (7). One obtains

$$\varepsilon_{xx} = \frac{\partial u}{\partial x} = \frac{1}{z}[z(1 - \lambda\cos\theta) - (\lambda\cos\theta)(\Delta z + x\frac{\partial \Delta z}{\partial x})] \tag{8}$$

$$\varepsilon_{yy} = \frac{\partial v}{\partial y} = \frac{1}{z}[z(1 - \lambda\cos\theta) - (\lambda\cos\theta)(\Delta z + x\frac{\partial \Delta z}{\partial y})] \tag{9}$$

$$\gamma_{xy} = \frac{\partial u}{\partial y} + \frac{\partial v}{\partial x} = -\frac{1}{z}(\lambda\cos\theta)(x\frac{\partial \Delta z}{\partial y} + y\frac{\partial \Delta z}{\partial x}) \tag{10}$$

## Experimental Proof for Generalized Moiré Gap Equation

Eq. (7) can be rearranged into

$$\Delta z = \frac{z}{\lambda\cos\theta}\left[(1 - \lambda\cos\theta) - \frac{u_r}{r}\right] \tag{11}$$

There exists a gap $\Delta z_{critical}$ (for $\lambda < 1$ only) at which the displacement $u_r$ is equal to zero. The sign of $u_r$ is determined by the term $(1-\lambda\cos\theta)$. They are of opposite sign when $\Delta z < \Delta z_{critical}$ and of same sign when $\Delta z > \Delta z_{critical}$. They are also of opposite sign for $\lambda \geq 1$.

The validity of eq. (11) was proved experimentally for cases where $\lambda = 1$ and $\theta = 0$ in reference [5] and [6]. In this study evidence will be given for cases where mismatches are included. In order to simplify the experiment constant gaps were used throughout, and linear and rotational mismatches were introduced separately. Therefore for $\lambda = 1$ eq. (11) reduces to

$$\Delta z = \frac{z}{\cos\theta}\left[(1 - \cos\theta) - \frac{u_r}{r}\right] \tag{12}$$

and for $\theta = 0$ it reduces to

$$\Delta z = \frac{z}{\lambda}\left[(1 - \lambda) - \frac{u_r}{r}\right] \tag{13}$$

To test the validity of eq. (12), two 8" x 10" plate gratings of 300 lines per inch were given a uniform gap of $z = 0.128" \pm 0.001$ and a rotational mismatch of 0°, 1°, 12', 2°9', 3°12' and 5°6' consecutively. Pictures of the moire patterns for which $\theta = 0°$, $\theta = 2°9'$, and $\theta = 5°6'$ are shown in Fig. 2. The displacement curves for all the five cases are plotted in Fig. 3 as fringe orders vs. r cos θ. The centers of fringes were accurately located with a microdensitometer. Care should be exercised in ordering these fringes[4]. In essence it is necessary to observe the condition that when $r = 0$, $u_r$ must also be zero because at the optical axis

there is no perspective effect. Successively increasing orders should be assigned to fringes in the increasing direction of r until a change of sign of the deviation of the displacement is encountered[7]. The starting order can be arbitrary but the abscissa of the plotted displacement curve should be shifted to accommodate the condition (i.e. $u_r = 0$ when $r = 0$). The average gap computed from eq. (12) using the information from Fig. 3 given an average value of 0.128 which agrees quite well with the actual gap.

For testing the validity of eq. (13), two 8" x 10" plate gratings of 300 and 296.23 lines per inch, respectively, were used. The value of $\lambda$ depends upon which of the two gratings is used as master (which is defined here as the one closer to the camera). If the former is used $\lambda = 1.0126$, and if the latter is used $\lambda = 0.9874$. For $\lambda = 1.0126$ cases of $\Delta z = 0.59" \pm 0.001"$ and $\Delta z = 0.123" \pm 0.001"$ and for $\lambda = 0.9874$ a case of $\Delta z = 0.064" \pm 0.001"$ were tested. Z was kept constant at 38.8" for all the three cases. Moiré patterns for $\lambda = 1.0126$ and $\Delta z = 0.059 \pm 0.001$, and $\lambda = 0.9874$ and $\Delta z = 0.064 \pm 0.001$ are shown in Fig. 4. It is interesting to note the difference in fringe densities in these two patterns. Had $\lambda$ been the same for both cases the fringe density would have been higher for the case where the gap was larger. The fact that larger gap rendered less fringes was due to the exchange of roles played by the two gratings.

Same procedures were used to plot the displacement curves which are shown in Fig. 5. The computed gaps from these curves using eq. (13) are the following: 0.064 for $\lambda = 1.0126$ and 0.059 and 0.123, for $\lambda = 0.9874$. The agreement is again very good.

## Deflection Measurements Using Moiré Gap Equation

The original motivation for the derivation of the moiré gap equation was to know the influence of a gap on the moiré pattern from which strain distributions were to be derived [4]. The gap between the gratings was created either by the out of plane deformation of the model grating under plane loading or due to uncontrolable circumstances under which the master grating had to be kept away from the model [8]. Now if one reverses the situation whereby a gap is created by the deflection of a model grating due to transverse loading, the gap equation can then be used as a means to compute the deflection at each and every point of the model. Indeed eq. (12) can be written as:

$$\Delta Z = A \frac{u}{r} + B \qquad (14)$$

where A and B are constants for a given experimental set-up. The simplest form of the equation of course is when the initial mismatches are zero (i.e. $\lambda = 1$ $\theta = 0$). However, there may be cases in which the responses are small so that an initially introduced mismatch pattern would be helpful in plotting the displacement curves.

In order to demonstrate the applicability of the moiré gap equation for deflection measurement a cantilever beam made of Plexiglas was used. The beam was printed with a grating of approximately 300 lines per inch with lines perpendicular to the longitudinal direction of the beam. The cross-section of the beam was 1/4" x 1/4" and a notch at 6" from the fixed end was cut on the beam to facilitate the application of load. The overall length from the fixed end was 6 3/4". A master grating plate of 300 lpi was in direct contact with the beam before loading. There was an initial pattern due to the

mismatch of line densities. Under loading the pattern changed because of the presence of gap between the two gratings. As demonstrated in Ref. [6] the appearance of the pattern depends on the location of optical axis. For this particular case moiré patterns for two locations of optical axis (one at the center and one at the fixed end of the beam) under different loadings were recorded. In Fig. 6 the moiré pattern under a load of 0.2281 lb for two optical axis locations are shown. Fringe were properly ordered and displacement curves are then plotted from the moiré patterns, for example, as shown in Fig. 7 where displacement curves correspond to the moiré patterns in Fig. 6. As mentioned earlier there was some initial linear mismatches between the two gratings. In computing deflections one could use eq. (13) with the computed $\lambda$ from the initial moiré pattern. An alternative, however, is to compute deflection using $\Delta z/z = u/r$ and then shift the abscissa to accommodate the boundary condition that the deflection is zero at the fixed end.* In doing so one need not know $\lambda$ and also saves some time in computation. The latter approach was adopted in the analysis and the results for four experiments plotted in dimensionless form are shown in Fig. 8. The agreement with the theoretical deflection curve is good.

As a second example, the problem of a circular plate with fixed boundary and loaded centrally with a concentrated force was chosen. The thin (1/16 inch) plate was also made of Plexiglas and clamped between two thick aluminum plates with a circular opening of 7 inch in diameter. The concentrated load was applied via a pin-hook with a head of 1/8 inch in diameter cemented to the bottom side of the plate. The plate was printed with a grating of 300 lpi and the master (a 8" x 10" glass plate) grating of identical line density was placed atop the aluminum plate with lines parallel to that of the model

---

*In general this cannot be done unless $\lambda \cong 1$. In the present case $\lambda = 0.999$.

grating. The initial gap due to the aluminum plate created a dense pattern of parallel straight fringes. Two positions for the optical axis of the camera were also used for the experiments. One was at the center of the plate, and the other at the boundary and the shifting of optical axis was along the direction perpendicular to the grating lines. It should be noted that shifting of optical axis along the direction parallel to the grating lines will not effect the appearance of the patterns, because the perspective effect is unaltered under this condition. The initial moire' pattern of the plate as well as two patterns for a load of 2.18 lbs. but different positions of optical axis are shown in Fig. 9. In plotting the displacement curves fringe positions were again accurately located by microdensitometer tracings. A total of four experiments (for two positions of optical axis) were performed and the results of experimentally determined deflection curve along the diameter perpendicular to the grating lines together with the theoretical solution are shown in Fig. 10. The agreement is satisfactory but not as good as the previous case. One reason for the discrepency is due to the fact that while the theoretical deflection curve is for a concentrated load, the actual loading was distributed over a circular area of more than 1/8" in diameter. This may explain why that the experimental values were lower than the theoretical ones near the central region of the plate.

As a final example for the application of the method, a perforated square plate simply supported at two opposite corners and concentrately loaded at the center was used. While a problem of this kind is usually not easily accessible to analytical approaches it presents no special problem to whole-field experimental methods like the present one. The plate was also made of Plexiglas and its configuration is shown in Fig.11(a).

A grating of 300 lpi was printed on the bottom face of the plate with lines parallel to one edge. A glass master grating of same line density was laid on top of the plate with no rotational mismatch. The initial gap between the two gratings due to the thickness of the plate again created a moiré pattern. The moiré pattern under loading with optical axis at the center of the plate is shown in Fig. 11(b). Deflections along two sections (A-A & B-B) were computed. While usual procedures were used to compute the deflections along section A-A, some modifications were needed in computing deflections along section B-B. In computing deflections along sections that are not principal (i.e. sections perpendicular to the grating lines) it is necessary to take into account the fact that the effective pitch of the master grating along this section is $p/\cos\theta$, in which p is the pitch of the master grating and $\theta$ is the angle that the section deviates from the principal section*. The result of the computed deflection curves are shown in Fig. 12. No theoretical solution is available for comparison.

Conclusions and Discussions:

It may be concluded that the moiré gap equation can be effectively utilized as a means for the determination of deflections of structures under transverse loading. The method offers simplicity over the other optical methods: It does not require elaborate equipment (a camera and a master grating are sufficient) and the model used need not have a optical flat surface or a reflective surface. While one may argue that the necessity of printing lines on the plate is a drawback, it is worth noting that there are commercially available plastic plates with light-sensitive emulsion already coated (Kodak Photoplast Plates). Printing gratings on these plates is as easy as printing gratings on photographic films [9].

---

*An alternative leading to the same result is to use $r\cos\theta$ rather r in computing the distance.

It should be noted that in deriving the moiré gap equation the inclination effect of the model grating was not taken into account nor did the surface strains of the model under load. The effect of the inclination of the model grating was shown in Ref. [6] to be of no significance even for a slope of 0.0238. The effect of the surface strain seems to be of little significance judging from the close agreement between theoretical and experimental results for the cantilever beam. While it is evident that when the deflection becomes very large the errors will not be negligible it may be safe to say that within the limits of the small deflection theory of plates, the present method gives sufficiently good results.

Another use of the moiré gap effect is its applications to the vibration problems of beams and plates. For example, if a plate with a grating printed on its top surface is under a steady state vibration, and a master grating is placed over it with a certain gap so that it will not get into contact with the vibrating plate, the moiré pattern created by the gap effect will continuously change due to the changing gaps from point to point, except at those places where nodel points or lines occur. Therefore, if a camera is used to record the phenomenon with an extended exposure time, the pattern of nodel lines or points will be recorded as a portion of the original gap moiré pattern while the rest of the place washed out. Indeed if a high speed camera is used, it is also possible to determine the transient deflections of plates and beams.

Acknowledgement:

The research was accomplished under the financial support of the National Science Foundation through an Engineering Research Initiation Grant No. GK - 3039.

# REFERENCES


1. Dantu, P., "Utilisation des Resaux pour l'etude des Deformations" Laboratoire Central des Ponts et Chaussees, Paris, Publication 57-6, 1957.

2. Morse, S., Durelli, A.J. and Sciammarella, C.A., "Geometry of Moiré Fringes in Strain Analysis", J. of the Engineering Mechanics Division, Proceedings of the ASCE, Vol. 86, EM4, August 1960.

3. Sciammarella, C.A. and Durelli, A.J., "Moiré Fringes as a Means of Analyzing Strains" Transactions, ASCE Vol. 127, Part I, 1962.

4. Chiang, Fu-pen, "A Method to Increase the Accuracy of Moiré Method" J. of the Engineering Mechanics Division, Proceedings of the ASCE, Vol. 91, No. EM1, Feb. 1965.

5. Sciammarella, C.A. and Chiang, Fu-pen, "Gap Effect on Moiré Patterns" Zeitschrift für angewante Mathematik und Physik, Vol. 19, Fasc. 2, 1968.

6. Chiang, Fu-pen and Ranganayakamma, B., "Some Experimental Evidence for the Validity of Moire Gap Equation", to be published in Experimental Mechanics.

7. Chiang, Fu-pen, "Determination of Signs in Moiré Method" J. of the Engineering Mechanics Division, Proceedings of the ASCE, Vol. 95, No. EM6 December 1969.

8. Sciammarella, C.A. and Chiang, Fu-pen, "Dynamical Stresses and Strains in Propellant Grains" 6th Annual Mechanical Behavior Working Group Meeting of ICRPG, Jet Propulsion Laboratory, Pasadena, California, Dec. 1967, CPIA Publication No. 158, Vol. 1, October 1967.

9. Chiang, Fu-pen, "Discussion - Production of High-density Moiré Grids" Experimental Mechanics, Vol. 9, No. 6, June, 1969.

## Figure Captions

Fig. 1 Optical Arrangement for the Observation of Moiré Gap Effect

Fig. 2 Moiré Patterns due to Gap and Rotational Mismatch
a) $\theta = 0°$, $\Delta z = 0.128" \pm 0.001"$
b) $\theta = 2°9'$, $\Delta z = 0.128" \pm 0.001"$
c) $\theta = 5°6'$, $\Delta z = 0.128" + 0.001"$

Fig. 3 Displacement Curves for Moiré Patterns due to Gap ($\Delta z = 0.128" \pm 0.001"$) and Various Rotational Mismatches

Fig. 4 Moiré Patterns due to Gap and Linear Mismatch
a) $\lambda = 0.9874$, $\Delta z = 0.064" \pm 0.001"$
b) $\lambda = 1.0126$, $\Delta z = 0.059 \pm 0.001"$

Fig. 5 Displacement Curves for Various Combinations of Gap and Linear Mismatch
I - $\lambda = 0.9874$, $\Delta z = 0.064" \pm 0.001"$
II - $\lambda = 1.0126$, $\Delta z = 0.059" \pm 0.001"$
III - $\lambda = 1.0126$, $\Delta z = 0.123 \pm 0.001"$

Fig. 6 Moiré Patterns for a Cantilever beam under Load for Two Positions of Optical Axis

Fig. 7 Displacement Curves Corresponding to Moiré Patterns in Fig. 6

Fig. 8 Experimental and Theoretical Deflection Curves for the Cantilever Beam

Fig. 9 Moiré Patterns of a Circular Plate with Fixed Boundary and Concentrated Load at the Center
a) Initial Pattern
b) Pattern Under Load with Optical Axis at Center
c) Pattern under Load with Optical Axis at Left End.

Fig. 10 Experimental and Theoretical Deflection Curves for the Circular Plate

Fig. 11 a) Configuration of the Perforated Plate Under Concentrated Force at Center
b) The Corresponding Moiré Pattern

Fig. 12 Experimental Deflection Curves along Sections A-A and B-B of the Perforated Plate

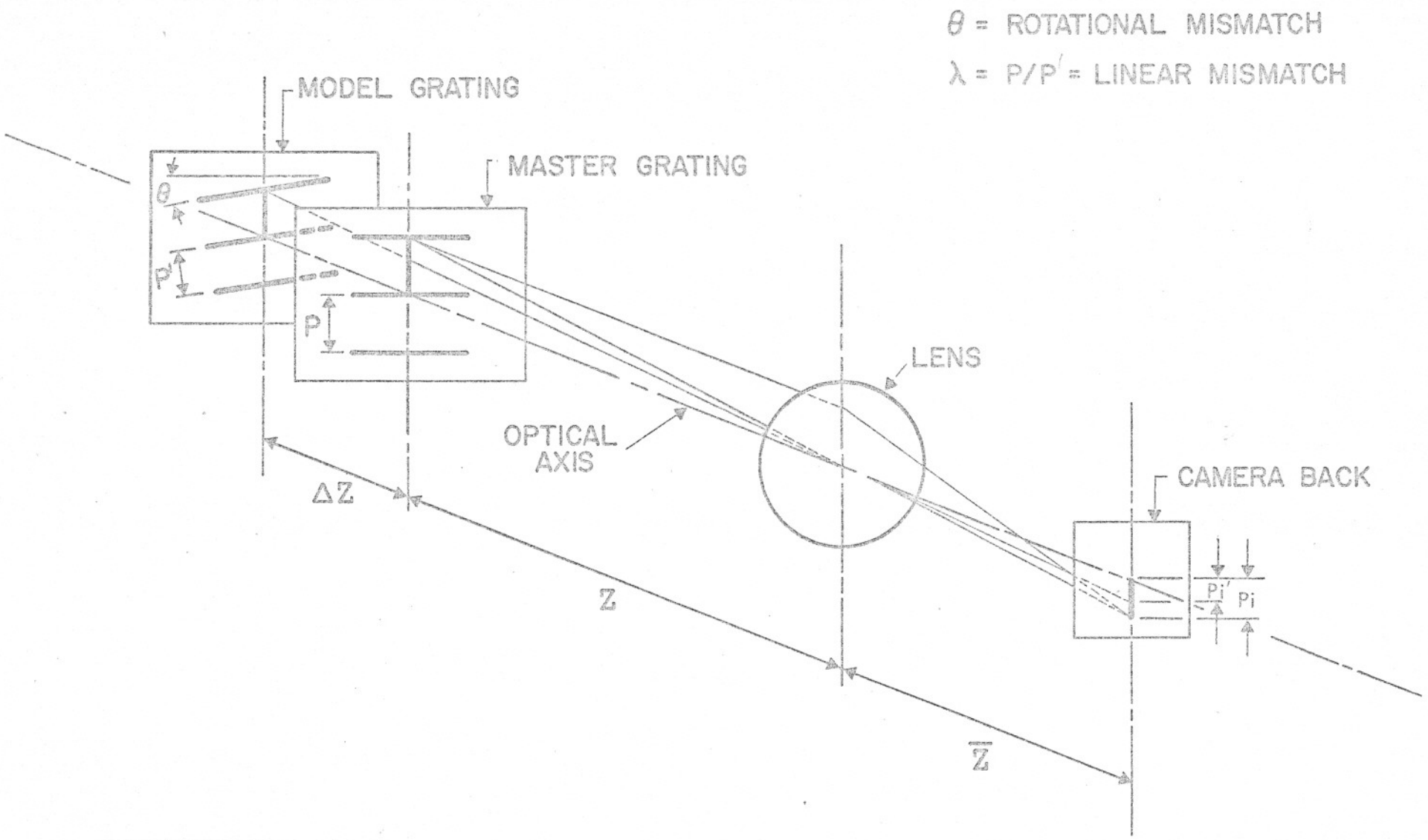


Figure 1 Optical Arrangement for the Observation of Moiré Gap Effect

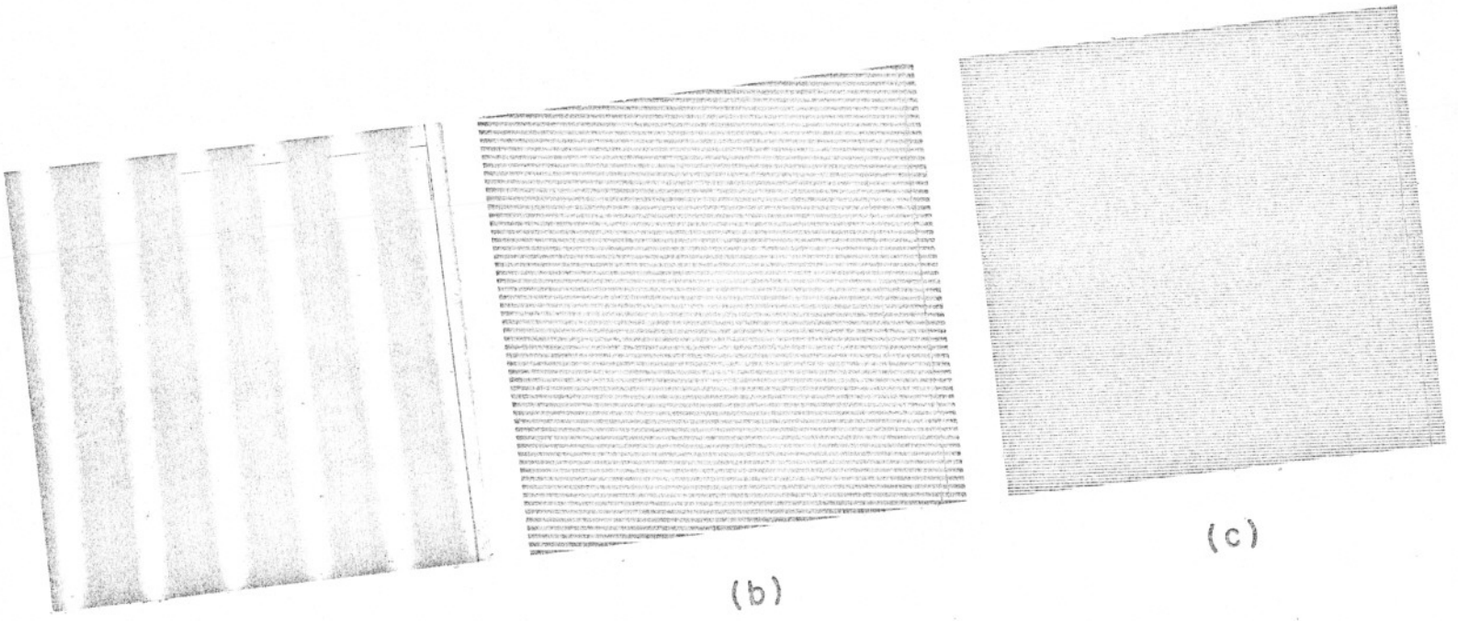


Fig. 2 Moiré Patterns due to Gap and Rotational Mismatch
a) $\theta = 0^{o}$, $\Delta z = 0.128" \pm 0.001"$
b) $\theta = 2^{o}9'$, $\Delta z = 0.128" \pm 0.001"$
c) $\theta = 5^{o}6'$, $\Delta z = 0.128" \pm 0.001"$

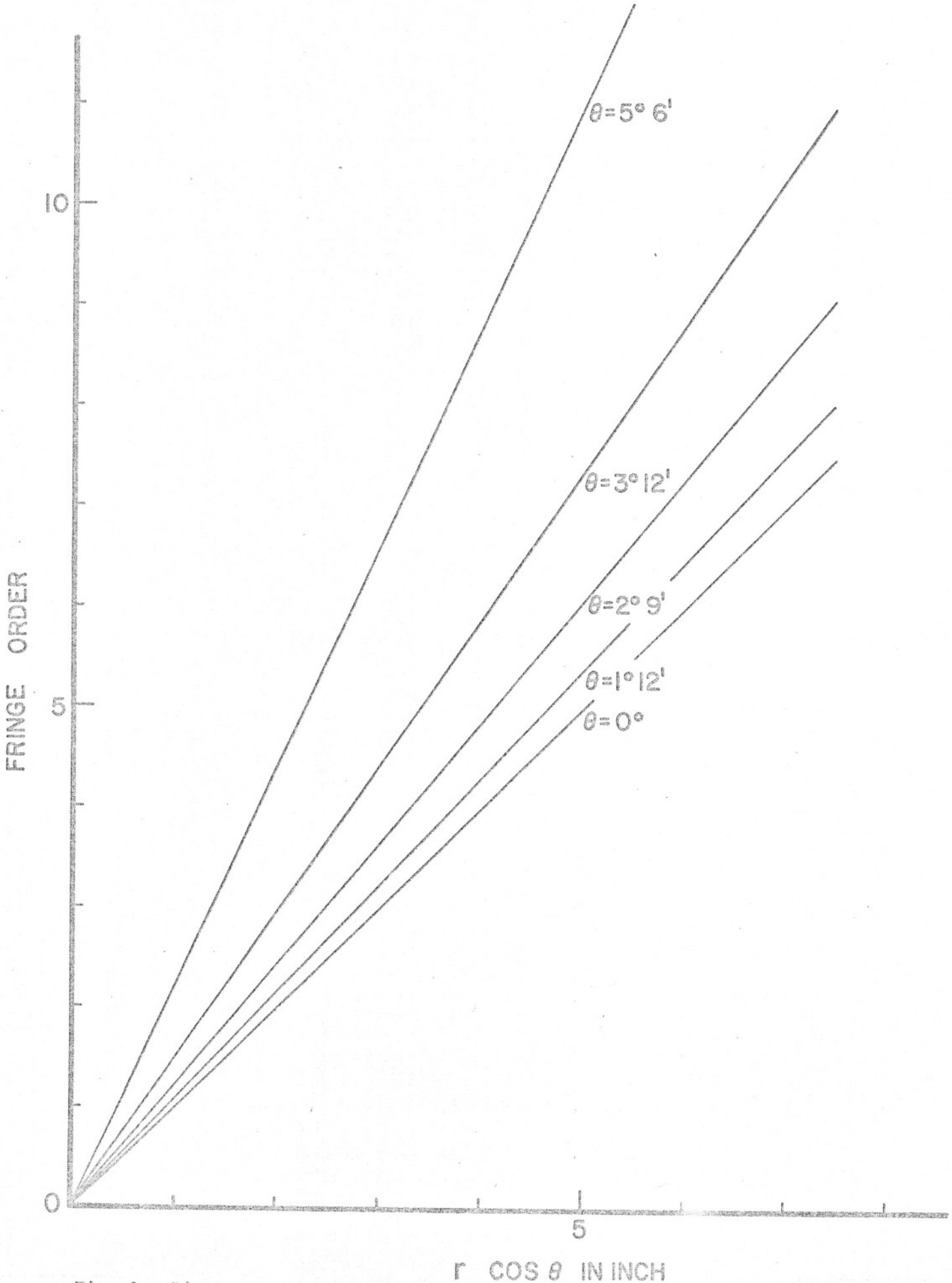


Fig. 3 Displacement Curves for Moiré Patterns due to Gap ($\Delta z$ = 0.128" ± 0.001") and Various Rotational Mismatches

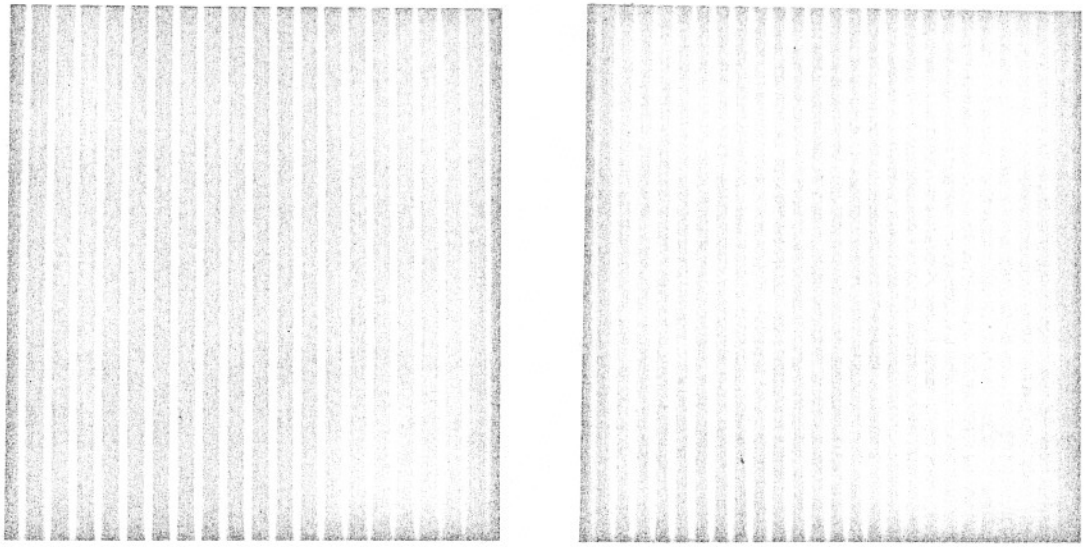

(a) (b)

Fig. 4 Moiré Patterns due to Gap and Linear Mismatch
a) $\lambda = 0.9874$, $\Delta z = 0.064" \pm 0.001"$
b) $\lambda = 1.0126$, $\Delta z = 0.059 \pm 0.001"$

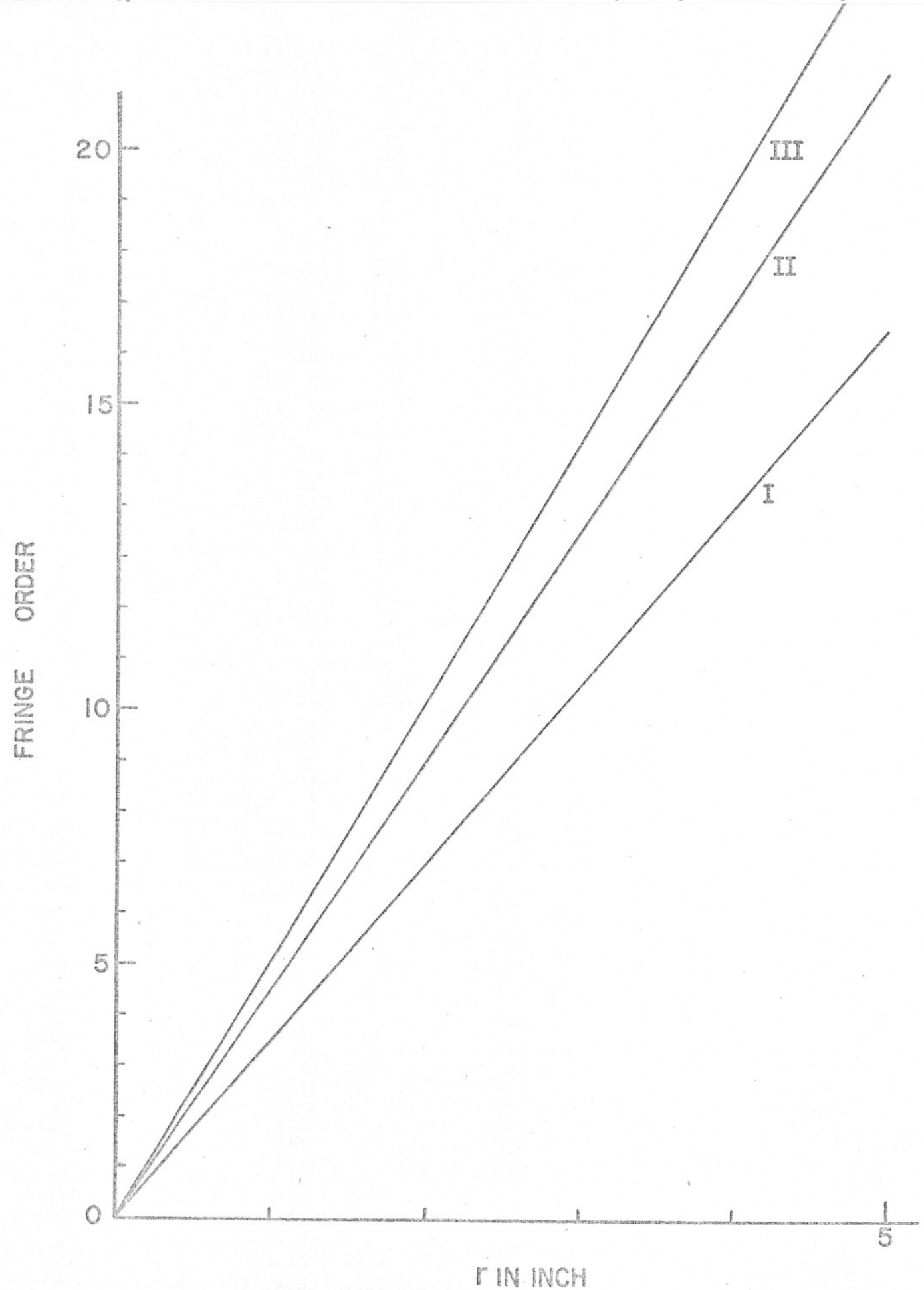


Fig. 5 Displacement Curves for Various Combinations of Gap and Linear Mismatch

I - $\lambda = 0.9874$, $\Delta z = 0.064" \pm 0.001"$

II - $\lambda = 1.0126$, $\Delta z = 0.059" \pm 0.001"$

III - $\lambda = 1.0126$, $\Delta z = 0.128 \pm 0.001"$

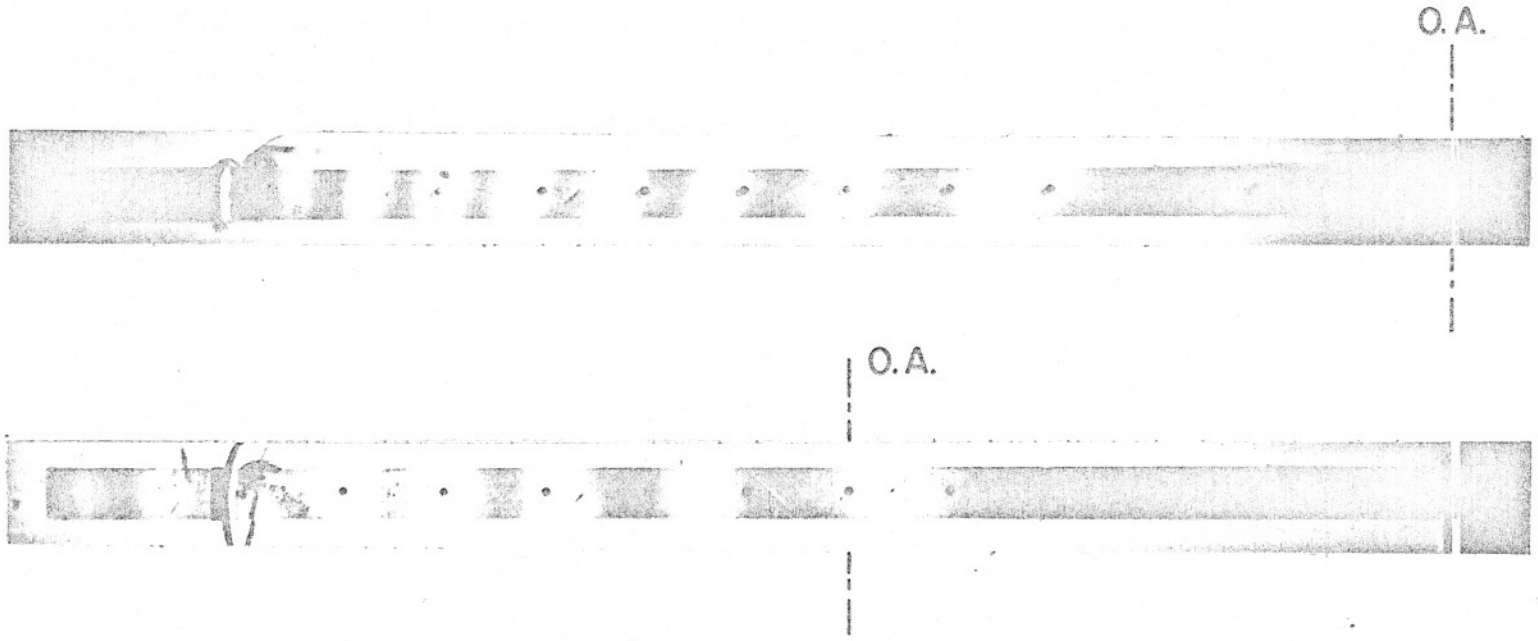


Fig. 6 Moiré Patterns for a Cantilever beam under Load for Two Positions of Optical Axis

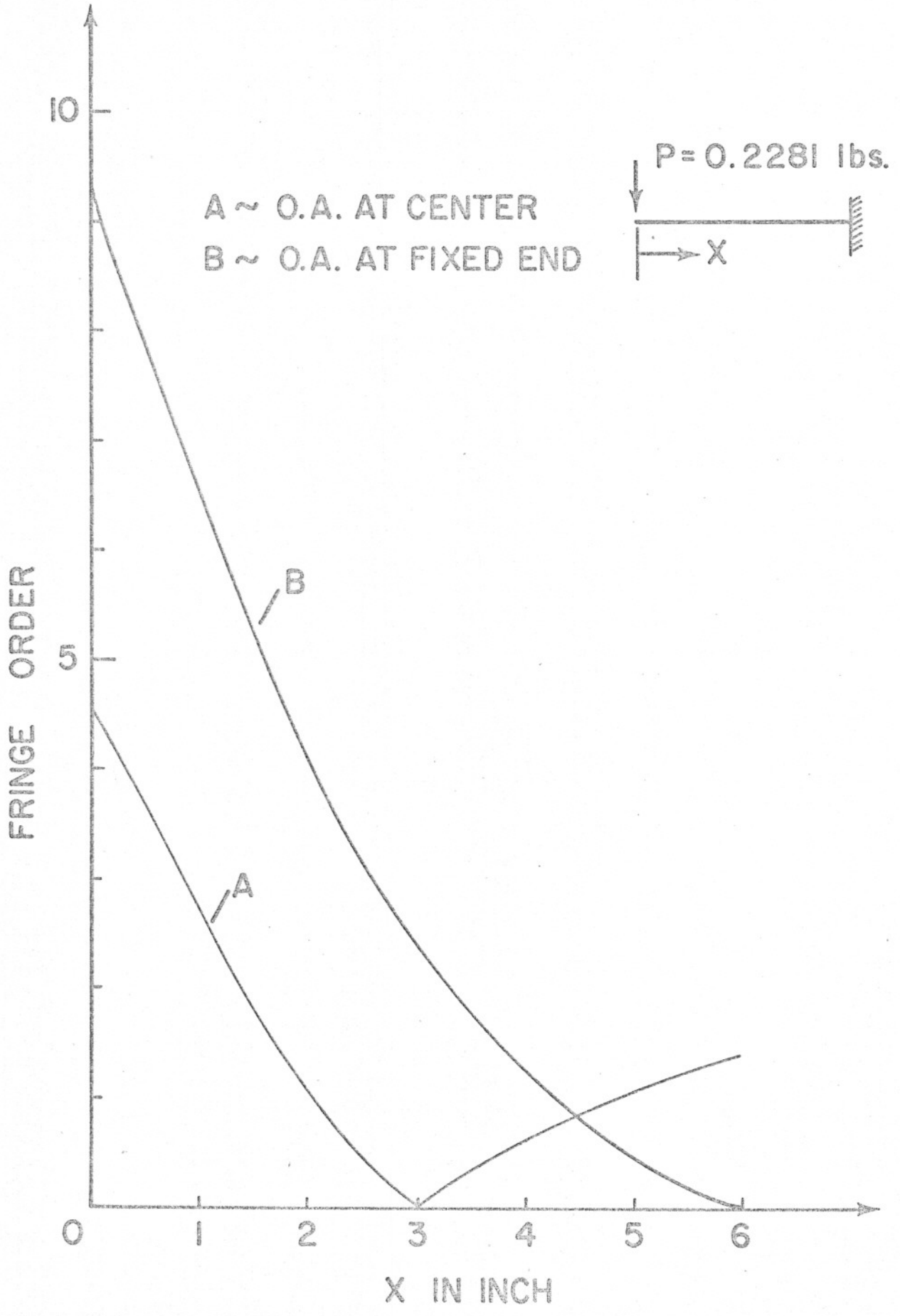


Fig. 7 Displacement Curves Corresponding to Moiré Patterns in Fig. 6

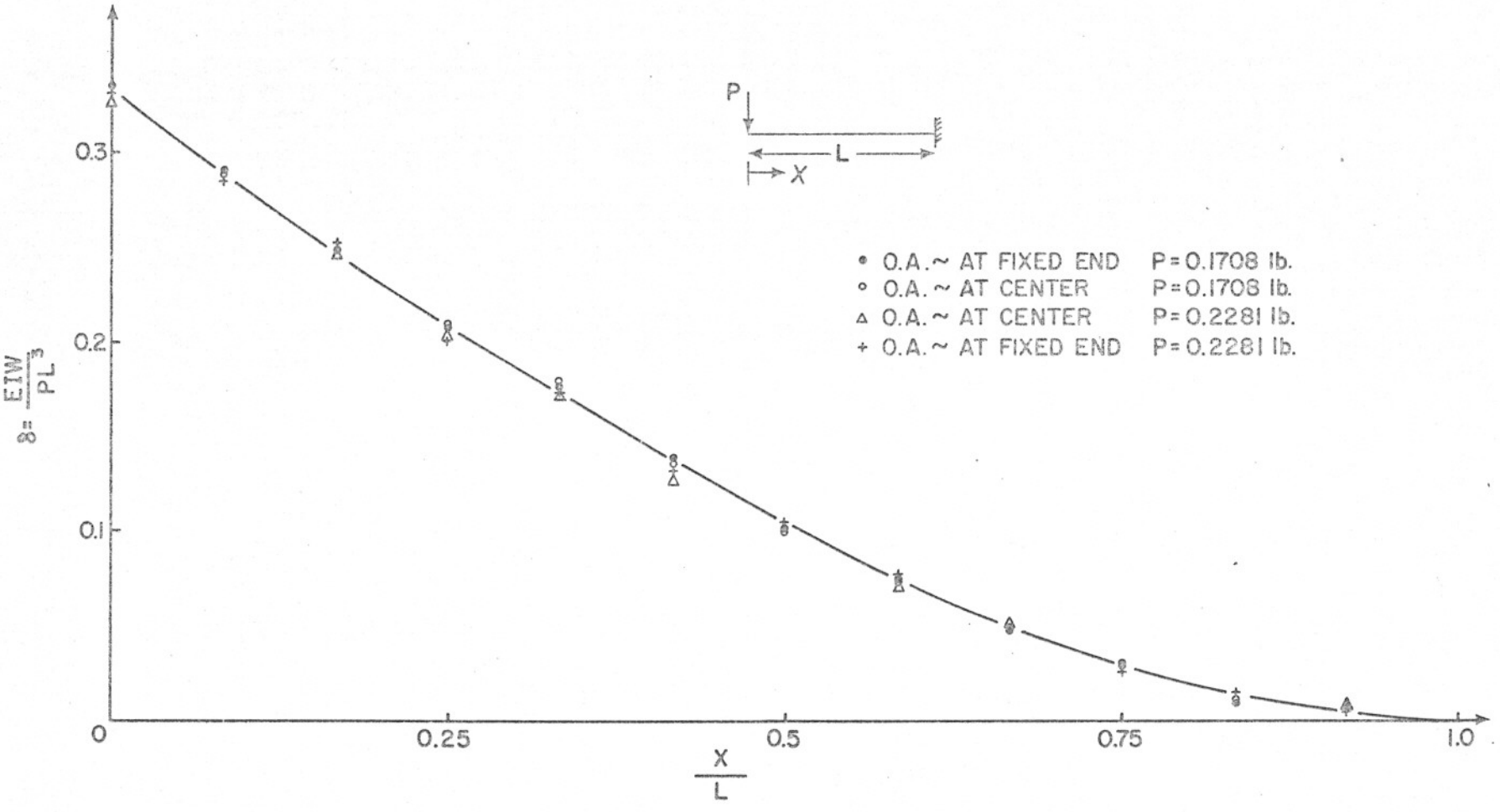


Figure 8 Experimental and Theoretical Deflection Curves for the Cantilever Beam

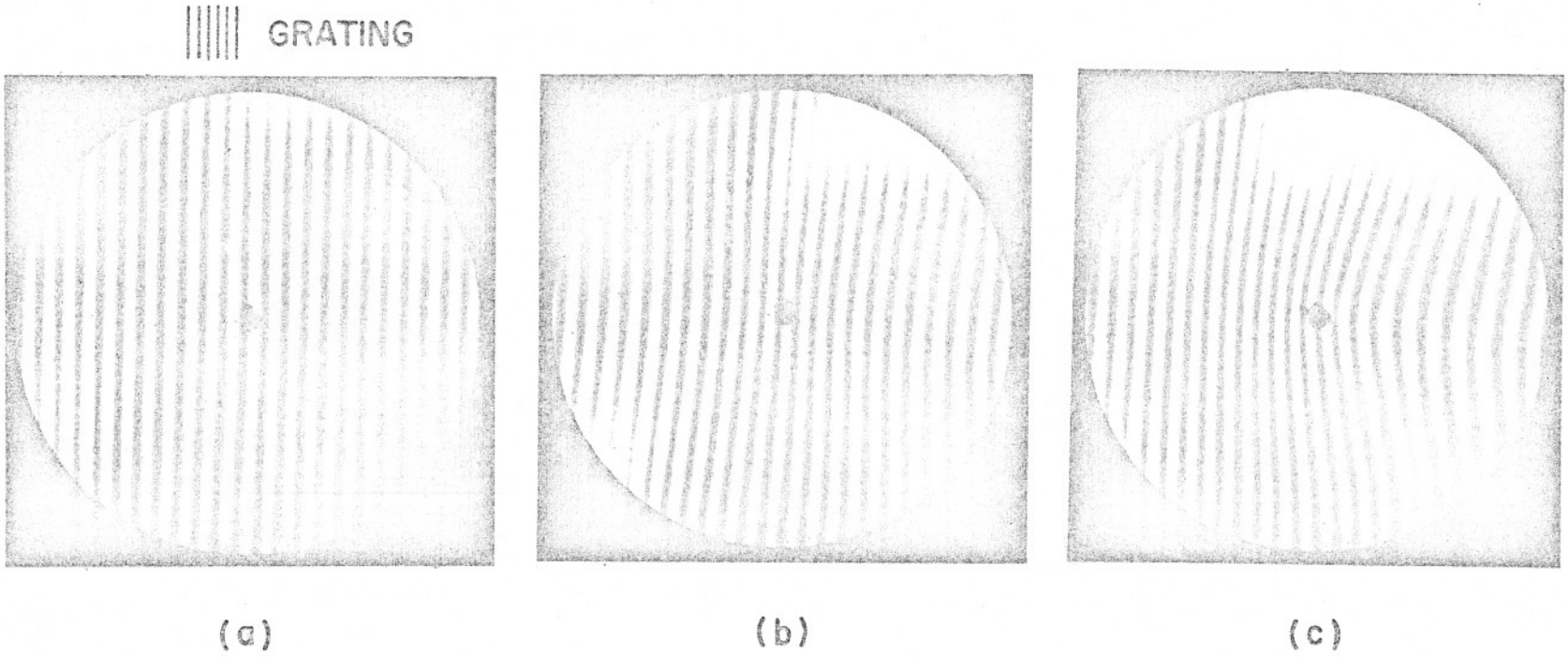


Fig. 9 Moiré Patterns of a Circular Plate with Fixed Boundary and Concentrated Load at the Center
a) Initial Pattern
b) Pattern Under Load with Optical Axis at Center
c) Pattern under Load with Optical Axis at Left End.

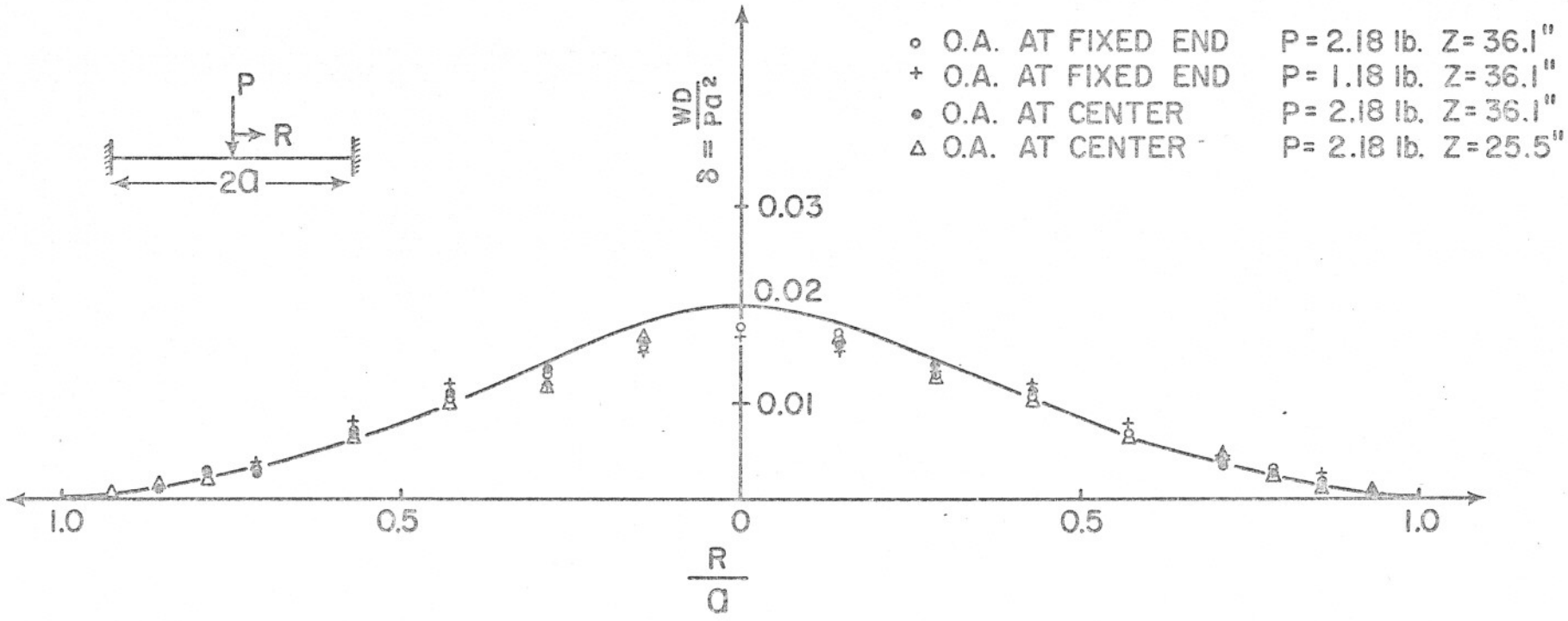


Fig. 10 Experimental and Theoretical Deflection Curves for the Circular Plate

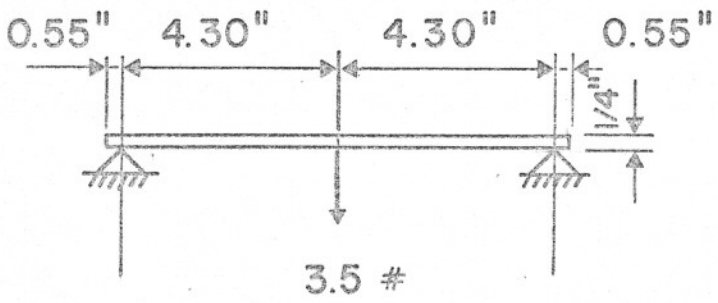


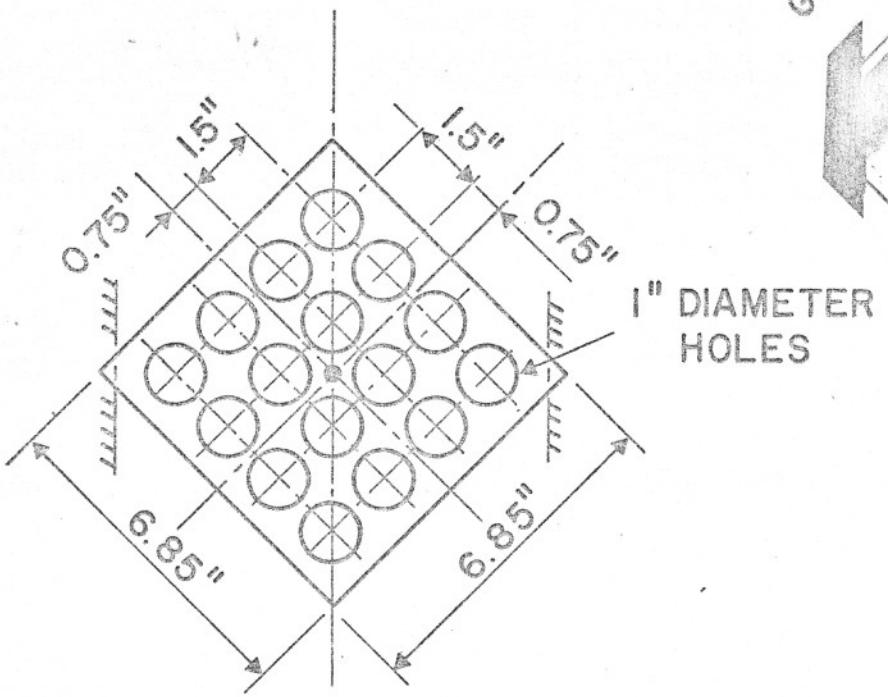


(a)

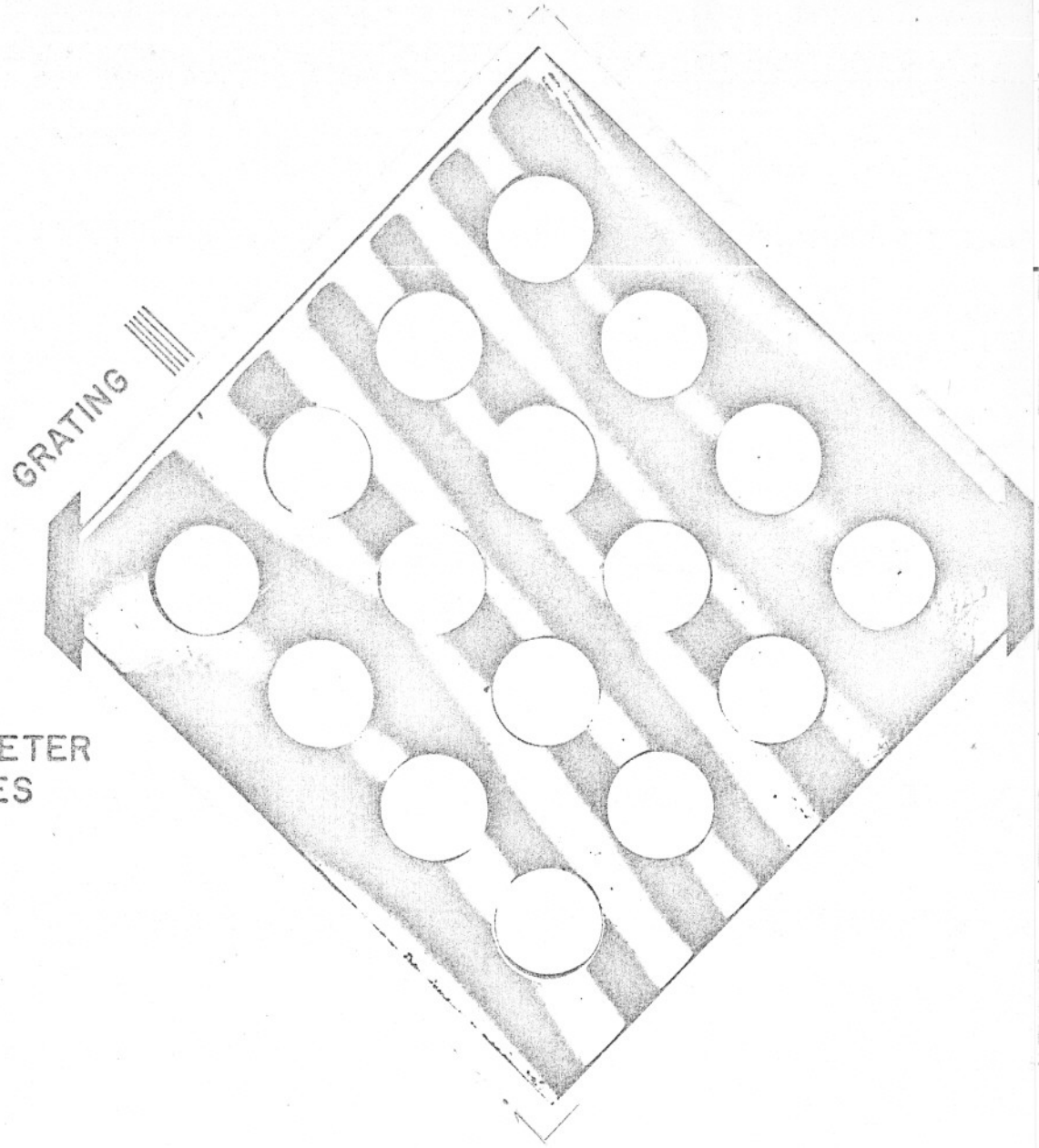


(b)

Fig. 11 a) Configuration of the Perforated Plate Under Concentrated Force at Center
b) The Corresponding Moiré Pattern

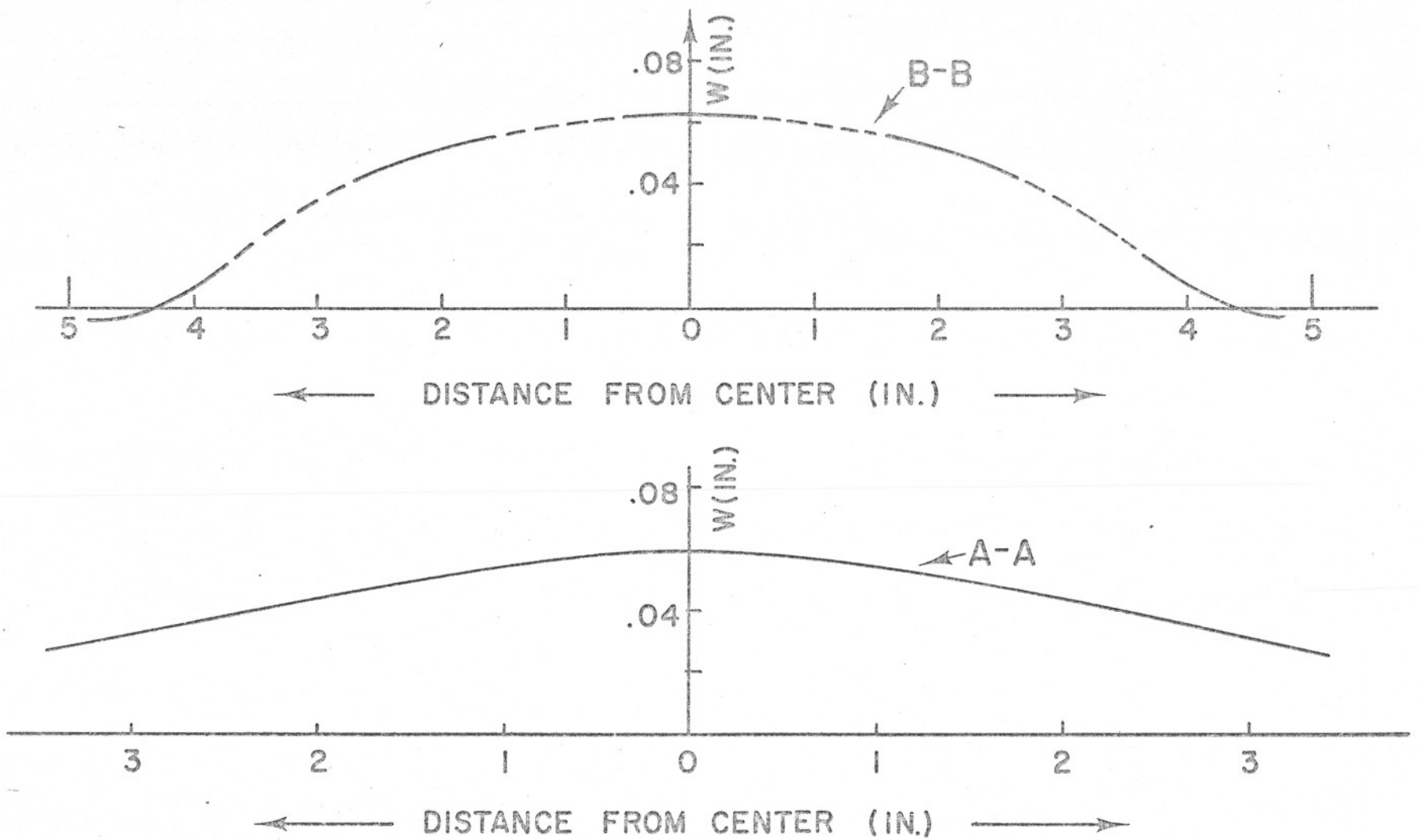


Fig. 12 Experimental Deflection Curves along Sections A-A and B-B of the Perforated Plate